ELECTRONIC SUPPLEMENTARY INFORMATION (ESI)

Nano ZnO decorated $ZnSnO_3$ as efficient fillers to PVDF: toward simultaneous enhancement of energy storage density and efficiency and improved energy harvesting activity

Abhishek Sasmal[1], Samar Kumar Medda[2], P. Sujatha Devi[3], Shrabanee Sen[1,*]

[1]Functional Materials and Devices Division, CSIR-Central Glass & Ceramic Research Institute, Kolkata-700032, India

[2]Specialty Glass Technology Division, CSIR-Central Glass & Ceramic Research Institute, Kolkata-700032, India

[3]Chemical Sciences and Technology Division, CSIR-National Institute for Interdisciplinary Science and Technology, Thiruvananthapuram-695019, India

*E-mail: shrabanee@cgcri.res.in

Discussion S1

Experimental

Raw materials

Following raw materials were used during the experiments of present work. Zinc acetate dihydrate [$Zn(CH_3COO)_2.2H_2O$] (Sigma Aldrich), tin (IV) chloride pentahydrate [$SnCl_4.5H_2O$] (LobaChemie, 98%), sodium hydroxide pellets [NaOH] (Merck, ≥ 97%) and distilled water were employed for the hydrothermal synthesis of untreated $ZnSnO_3$and $ZnO@ZnSnO_3$heterostructured particles. The PVDF based composite films were fabricated by using poly(vinylidene fluoride) (PVDF) powder (Sigma Aldrich, average M_W~534000 by GPC) and N,N-dimethyl formamide (DMF) [$HCON(CH_3)_2$] (Merck, ≥ 99%) along with as synthesized $ZnSnO_3$ or $ZnO@ZnSnO_3$ particles as starting materials.

Synthesis of $ZnSnO_3$ and $ZnO@ZnSnO_3$heterostructure

Hydrothermal technique was utilized in the present work. In a typical synthesis procedure of $ZnSnO_3$ (ZS), 0.096 gm of zinc acetate dihydrate and 0.154 gm of tin chloride pentahydrate were first added to 22 ml of distilled water (0.02 M solution of each material) in two separate 100 ml beaker and kept for magnetic stirring at room temperature. After ~5 min both the raw materials dissolved completely. Then the tin chloride (stannic chloride) solution was added to the zinc acetate solution slowly (dropwise) under magnetic stirring. Meanwhile 0.2 M NaOH solution was prepared by dissolving 0.176 gm of NaOH pellet in 22 ml of distilled water through magnetic stirring at room temperature. After ~10 min of mixing of zinc acetate and stannic chloride solutions, the NaOH solution was also added in it dropwise under continuous magnetic stirring at room temperature. The final mixture was kept for magnetic stirring for another 10 min at room temperature. The resulting solution was then transferred to a 100 ml

Teflon-lined stainless-steel autoclave and maintained at 130°C for 6 h. Then the autoclave was allowed to cool down naturally to room temperature. After that the white precipitate was collected by filtration through filter paper. During filtration process the precipitate was washed with distilled water several times until the pH become equal to 7. Then it was also washed with absolute ethanol twice and finally kept in an oven for drying at 80°C for 24 h. The ZnO@$ZnSnO_3$ heterostructure was also prepared by the same process (through in-situ growth) by using more amount of Zn-source. In this particular work we used 0.193 gm zinc acetate in 22 ml distilled water (0.04 M solution), 0.02 M stannic chloride solution and 0.2 M NaOH solution and followed the same technique as that in ZS to prepare ZnO@$ZnSnO_3$heterostructure (ZNZS).

Fabrication of PVDF ZS and PVDF-ZNZS composite films

To fabricate the PVDF based composite films of the synthesized ceramic particles, 0.49 gm of PVDF powder was first dissolved in 6 ml of DMF through magnetic stirring at 40°C for 2 h. Then the required amount of ceramic particles (0.026, 0.054 and 0.086 gm for 5, 10 and 15 wt% composite, respectively) were added to the PVDF solution (separately in different batches) and kept for magnetic stirring for ~48 h (to get homogeneous mixing). After every 12 h during this mixing, 30 min of bath sonication (50 W) was utilized for good dispersion. Finally, the mixed solution was drop casted on clean glass slides and kept in a dust free vacuum oven at 85°C for 4h. After annealing is completed, the slides were taken out of the oven and cooled down to room temperature. Then the resulting film (~0.07 mm thick) was peeled from the glass substrate and preserved for further characterization. 5, 10 and 15 wt% ZS filler loaded PVDF films were named as 5ZS, 10ZS and 15 ZS and the same for ZNZS filler loaded PVDF films were named as 5ZNZS, 10ZNZS and 15ZNZS, respectively. For comparison purpose, a pure PVDF film without adding any filler was also developed by the same technique.

Fabrication of energy storage and nanogenerator device

For electrical measurements, both sides of all the composite films were coated with high quality silver paste for electroding purpose. Then to fabricate piezoelectric nanogenerator device, both the electrodes were connected with copper wires. The copper wires were further connected with oscilloscope leads to the study of output ac signals. Further the piezoelectric nanogenerator (PENG) was used to develop hybrid piezoelectric-triboelectric nanogenerator (HNG) by using the following steps. Two piezoelectric films (one 10Zs and one 10ZNZS) of dimension 30×20×0.07 mm^3 were cut. One side of each film was electroded with high quality silver paste. The other side of the two films, where there was no electrode, was kept fixed face to face separated by PVDF spacer. HNG was now developed; two copper wires were connected with the two electrodes for output signal measurements. Before energy harvesting and sensing characterizations, both the PENG and HNG device was kept encapsulated inside a zip packet in order to protect it from vibrations which were applied over the surface during testing.

Characterization

X-ray diffraction (XRD) by using X'pert Pro MPD XRD system (PAN analytical) was utilized to study the crystal structure of ZS and ZNZS particles. The morphology of these particles was investigated by Field Emission Scanning Electron Microscopy (FE-SEM) (SEM Supra 35VP, Carl Zeiss, (accelerating voltage of 10 kV) and Transmission Electron Microscopy (TEM) (Tecnai G2, 30ST instrument (300 kV)). The HRTEM (High Resolution TEM) of decorated ZnO nanoparticles was studied by the same instrument. The elemental compositions of the synthesized nanoparticles were studied by Energy Dispersive X-Ray Spectroscopy (EDS) which was attached with TEM instrument. The information about the crystalline phases of PVDF and the composite films were investigated by employing a

Grazing Incidence X-ray Diffraction (GIXRD) (Rigaku) equipment. For detail phase investigation of the composite films, Fourier Transform Infrared Spectroscopy (FTIR) (FTIR-Spectrum 2, PerkinElmer) was used. A precession impedance analyzer (Wayne Kerr, 6500 B) was employed to study the room temperature dielectric properties of the composite films. The frequency dependent D-E hysteresis loop and electric field dependent current density of the composite films were investigated by RADIANT ferroelectric test systems (Radiant Technologies Inc.) using Vision software (Version 3.1.0). After applying different type of mechanical vibrations on the samples, the output electrical signal in terms of peak to peak ac voltage (V_{OC}) was studied by a Digital Oscilloscope (Tektronix, TBS 1072B). The output ac voltage was converted into dc by employing a bridge rectifier IC (DB 107) and the performance of that output dc voltage was demonstrated by charging a commercially available 10 μF capacitor. The d.c. voltage was measured by a FLUKE 115 True RMS Multimeter.

Fig. S1

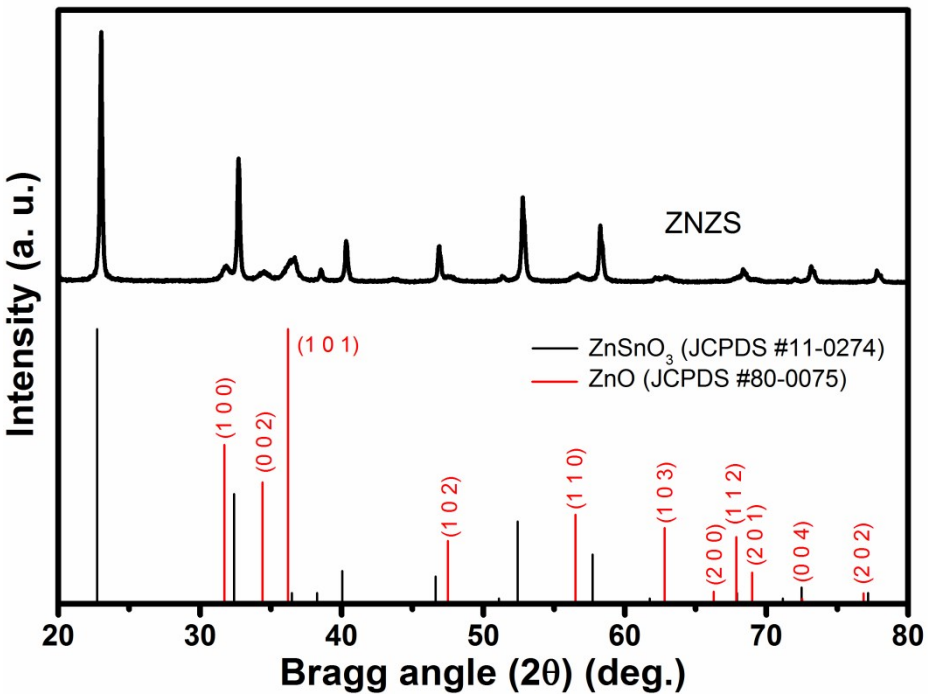

Fig. S1 Indexed XRD pattern of ZNZS sample.

Fig. S2

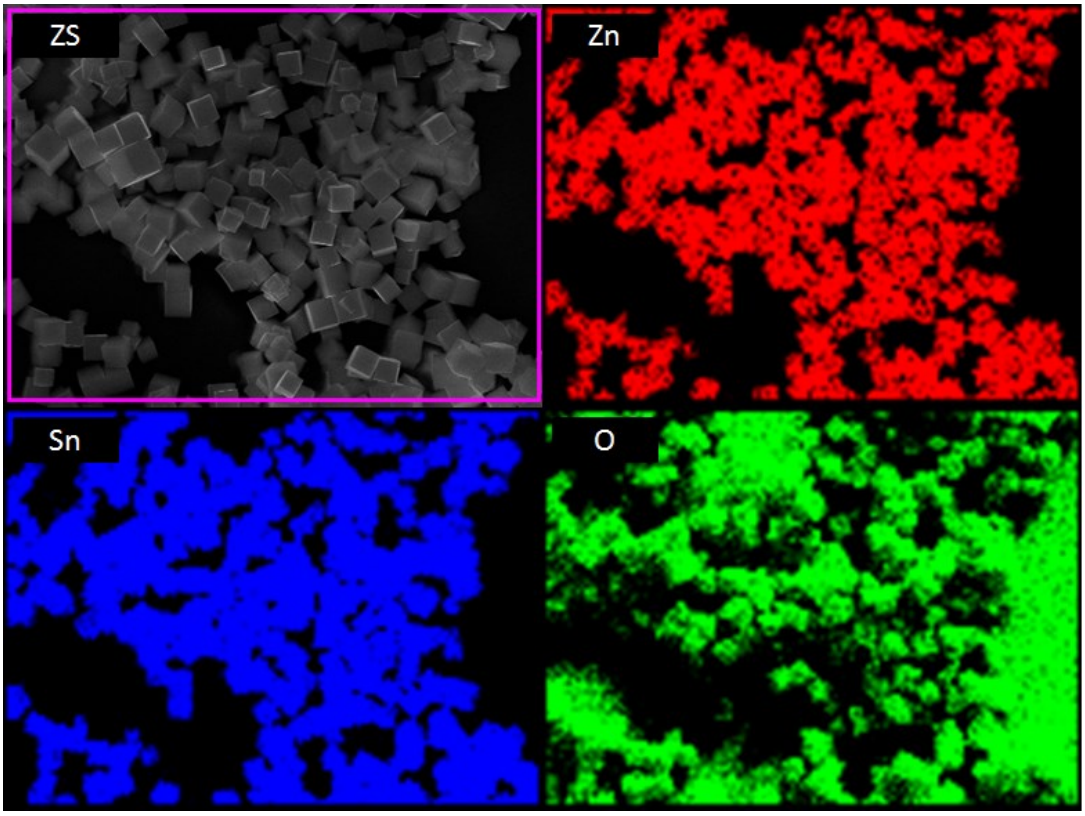

Fig. S2(a) EDS mapping of ZS particles.

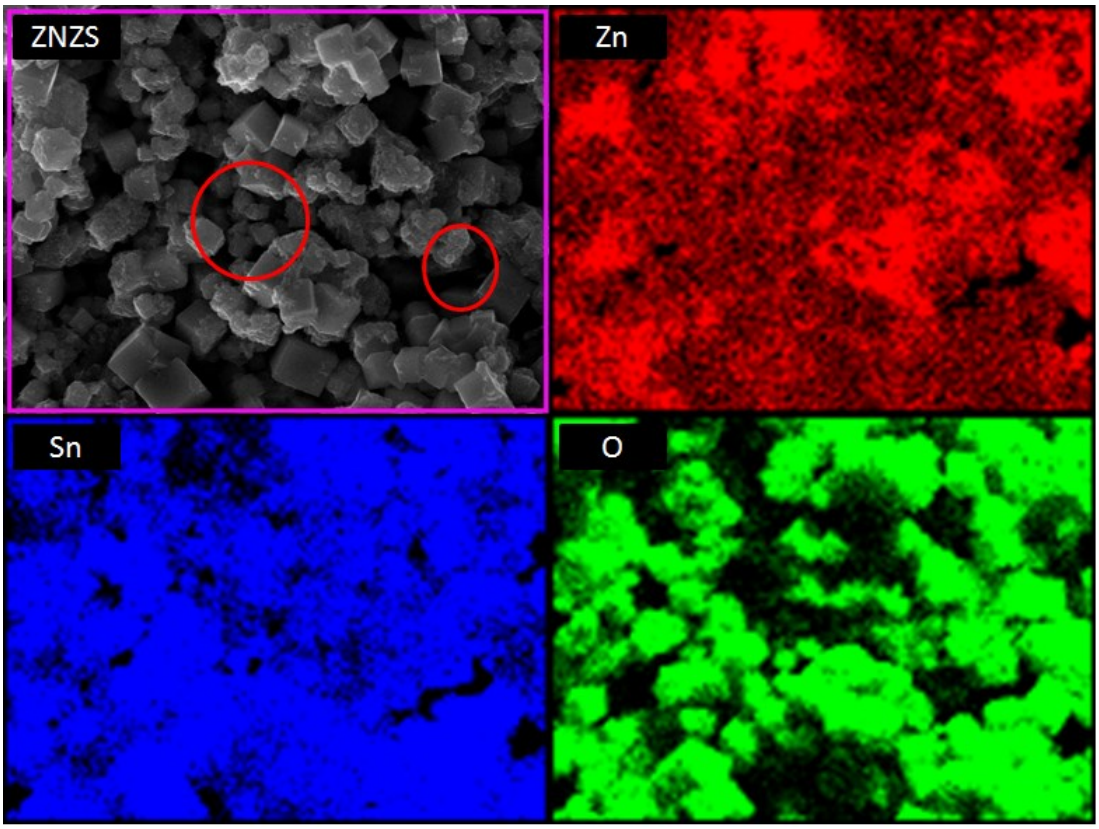

Fig. S2(b) EDS mapping of ZNZS particles.

Discussion S2

The EDS mapping of ZS and ZNZS particles were studied by FESEM instrument. Fig. S2(a) presents the EDS mapping of ZS particles which indicates that the elemental points corresponding to Zn and Sn are only confined to the cubic shaped region of ZS particles. The elemental points corresponding to O are also present in the said region. Additionally some signals corresponding to O are also observed due to the glass substrate (SiO_2). As the substrate contained oxygen, during elemental quantification, only the proportion of Zn and Sn was considered. The calculated proportion of Zn and Sn was found to be 52:48 (Zn:Sn) (shown in Table S1) which almost matched with the desired proportion.

The EDS mapping of ZNZS particles is shown in Fig. S2(b). Though it is difficult to observe core shell type structure by FESEM EDS mapping, a close and careful observation of Fig. S2(b) (especially the red circled region of ZNZS) gave the idea about core shell structure. It is observed that the Sn points are distributed distinctly in some region of ZNZS. But the Zn points are distributed quite uniformly throughout the whole region of ZNZS. This was due to the fact that the Sn points are confined to cubic shaped ZS particles only. Whereas, the Zn points are present both in the cubic shaped ZS and in the deposited particles on ZS surface. This proves that the deposited particles are Zn-rich. Though the idea about oxygen could not be particularly observed due to SiO_2 substrate, the presence of points corresponding to O in the deposited particles outside cubic ZS helps us to assume that the deposited particles are ZnO. The proportion of Zn and Sn of ZNZS samples was found to be 66:34 (Zn:Sn) (shown in Table S1) which also supports our assumption.

Therefore, all these facts, the appearance of ZnO peaks in XRD of ZNZS and the appearance of ZnO planes in the HRTEM of deposited particles on ZS of ZNZS sample jointly confirmed that the deposited particles on ZS of ZNZS sample are ZnO only.

Table S1

Table S1 Atomic proportion of Zn and Sn of ZS and ZNZS sample obtained from FESEM EDS mapping.

Sample Name	Zn:Sn
ZS	52:48
ZNZS	66:34

Fig. S3

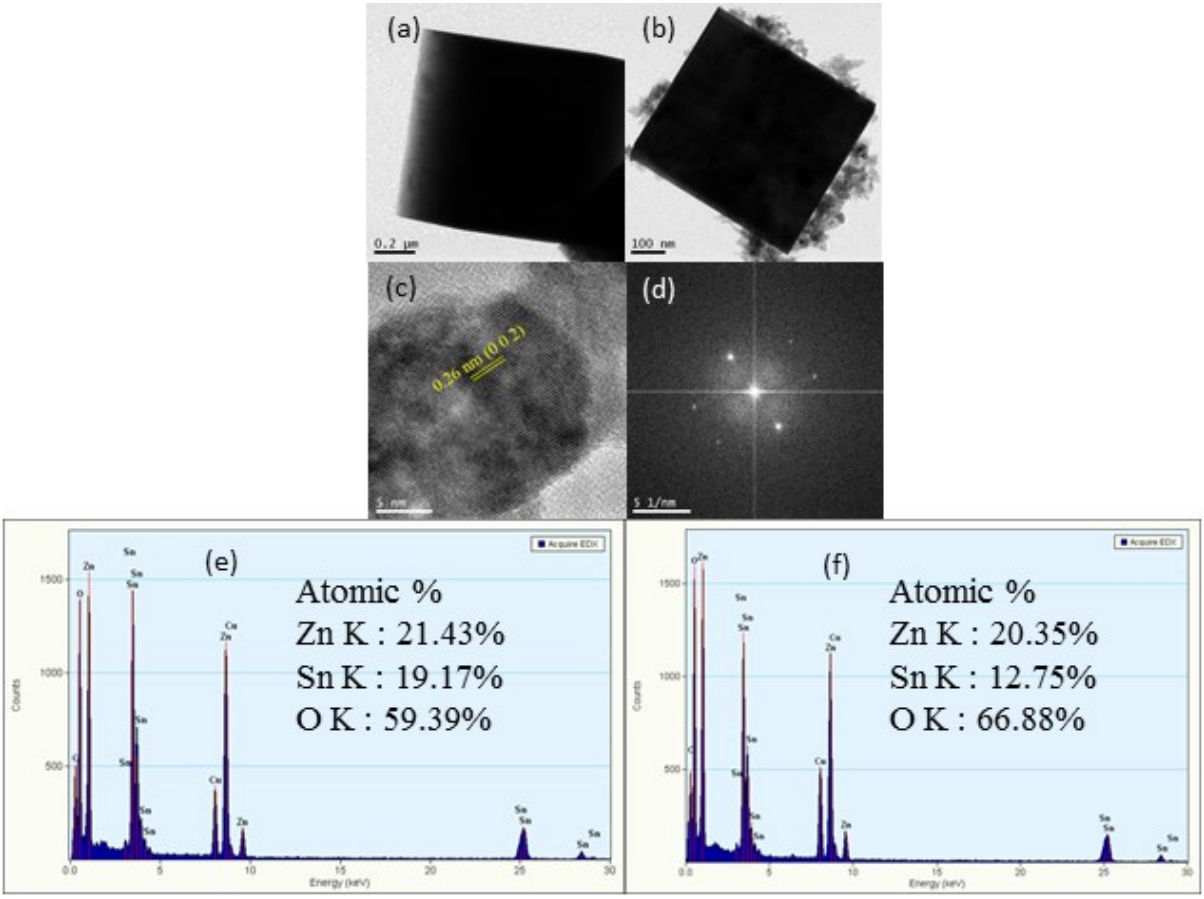

Fig. S3 Bright field TEM image of (a) ZS and (b) ZNZS particles. (c-d) HRTEM and corresponding FFT pattern of decorated ZnO particles, respectively. (e-f) EDS spectra of ZS and ZNZS particles, respectively.

Fig. S4

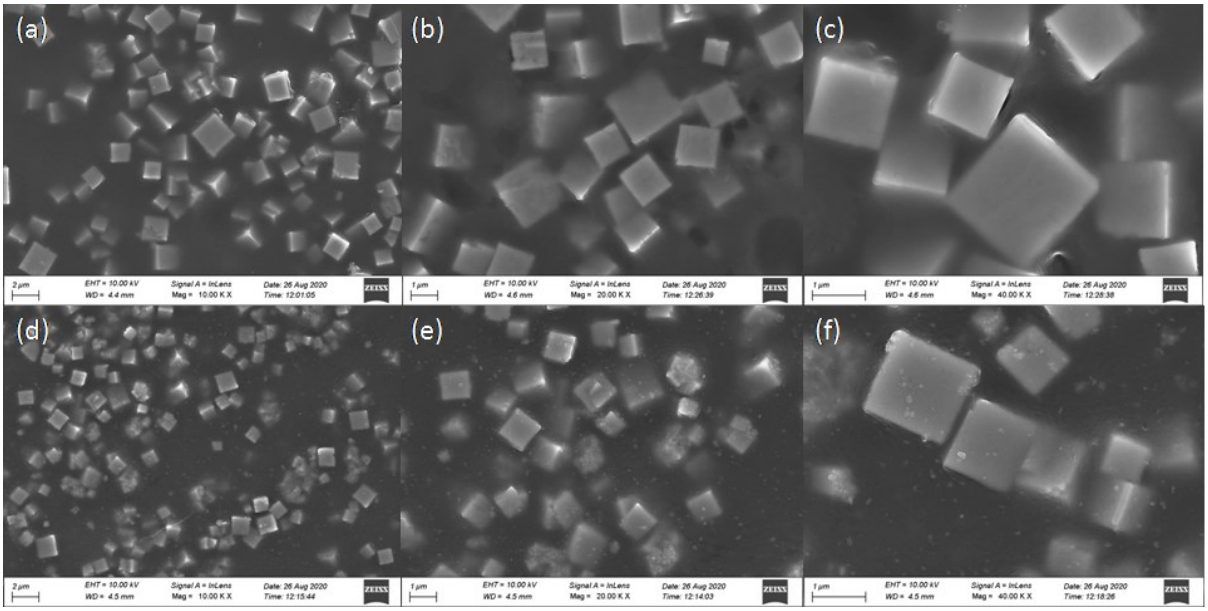

Fig. S4 FESEM images of (a-c) 10ZS and (d-f) 10ZNZS films at different magnifications.

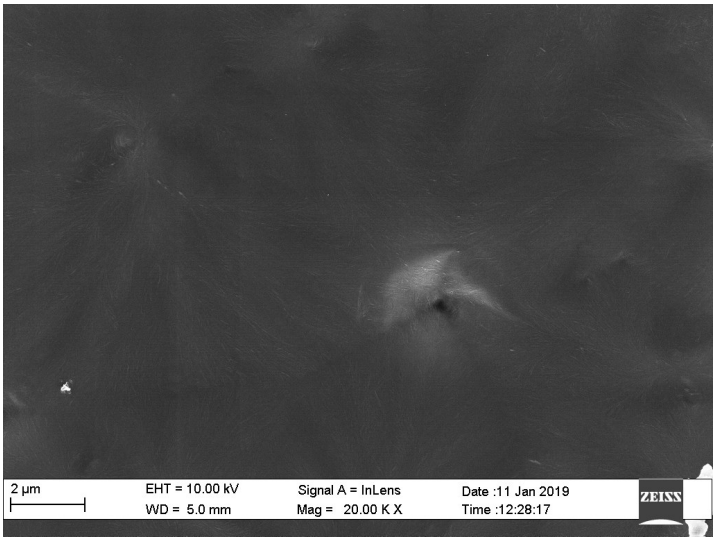

Fig. S4(g) FESEM image of bare PVDF film.

Fig. S5

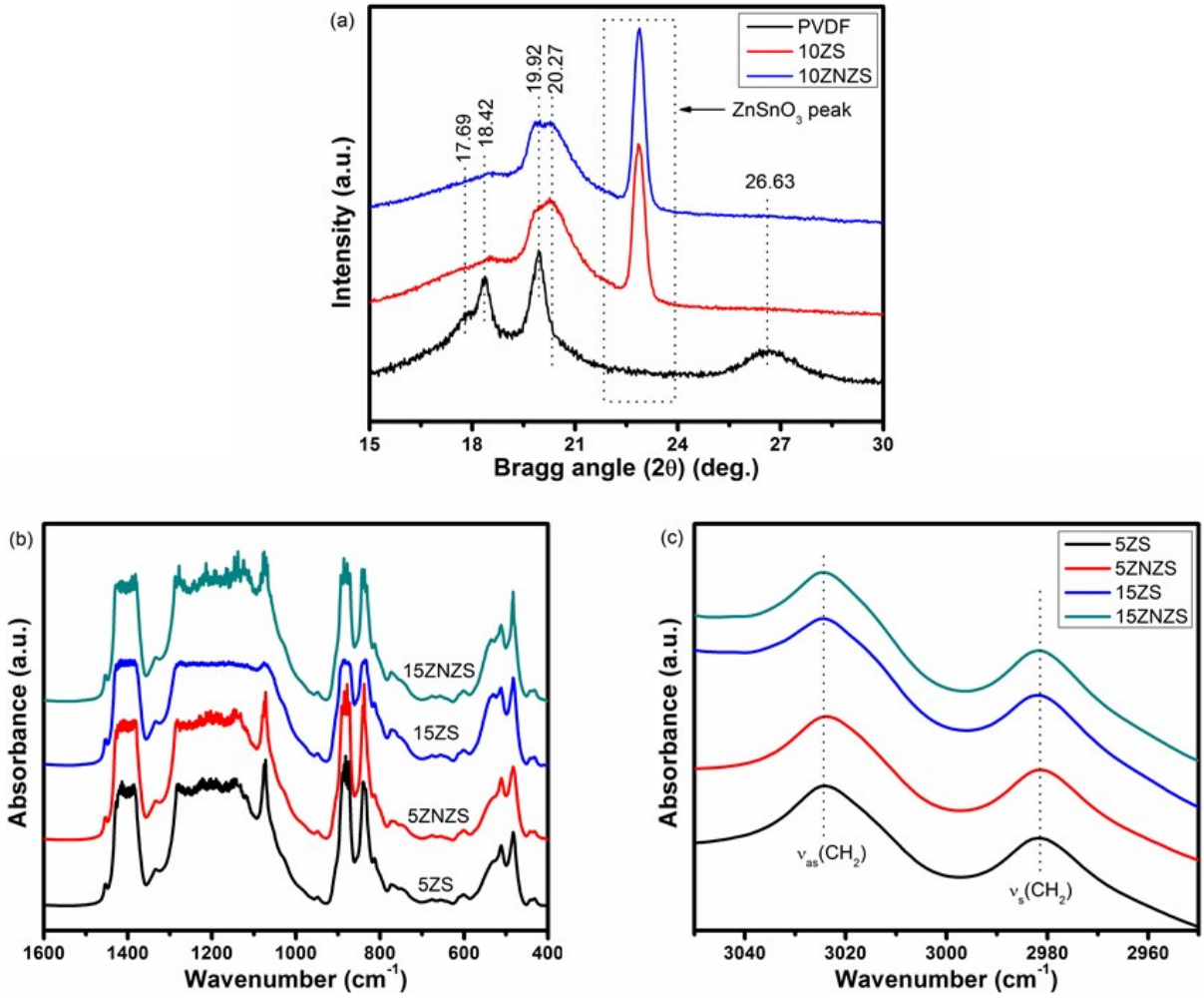

Fig. S5 (a) XRD pattern of PVDF, 10ZS and 10ZNZS films within the 2θ range of 15°-30°. FTIR absorbance spectra of 5ZS, 5ZNZS, 15ZS and 15ZNZS films with wavenumber ranging from (b) 1600 to 400 cm^{-1} and (c) 3100 to 2900 cm^{-1}.

Discussion S3

It is believed that the dielectric constant of PVDF based composite films, which is basically the charge holding capacity of the samples, is driven by different type of polarization mechanisms like, Maxwell-Wagner-Sillars (MWS) interfacial polarization, space charge polarization, orientational or dipolar polarization, etc. The frequency dependent dielectric permittivity curves as depicted in Fig. 6(a) showed the decrease in permittivity with increasing frequency which was mainly due to reduced MWS polarization and space charge polarization.[21]

All the loss curves showed same tendency of frequency response, first decreased with increasing frequency up to ~10 kHz, then it started increasing with increase in frequency. The increase in dielectric loss in the low frequency region (below ~10 kHz) was attributed to interfacial polarization and the increase in dielectric loss in the high frequency region was possibly due to the presence of glass transition relaxation of PVDF around 10 MHz.[21]

Another important observation from the dielectric loss curve was the lowest value of tan δ of PVDF in low frequency region but the highest value of tan δ for the same film at high frequency region. This result is probably attributed to the improved interfacial interaction of fillers with PVDF dipoles.[3] Along with the space charge polarization, polymer chain movement of PVDF is also a main source of its *tan δ*. When there was no filler loading in PVDF, its polymer chains were free to move in the whole experimental frequency region. But after inorganic ZS/ZNZS filler loading in the host PVDF matrix, interfacial electrostatic interaction of PVDF dipoles with ZS/ZNZS particle surface increased (seen earlier from XRD and FTIR characterizations of the composite films). Therefore, the movement of macromolecular polymer chains of PVDF was hindered by this improved interfacial interaction. Therefore, the dielectric loss was reduced. But in the low frequency region, there

was a strong effect of space charge polarization due to increased conduction pathway. Due the effect of this space charge polarization in low frequency region, the *tan δ* increased. In this frequency region, the increased space charge polarization probably had stronger effect than the effect of the suppression of polymer chain movement due to enhanced interfacial interaction. Therefore *tan δ* of ZS/ZNZS loaded PVDF films increased in the low frequency region. But the space charge polarization disappeared at the high frequency region. Therefore, at this frequency region the dielectric loss was only governed by the enhanced interfacial interaction. Therefore, the *tan δ* was observed to be reduced due to the hindrance of polymer chain movement caused by improved interfacial interaction of PVDF with ZS/ZNZS filler surface.

Fig. S6

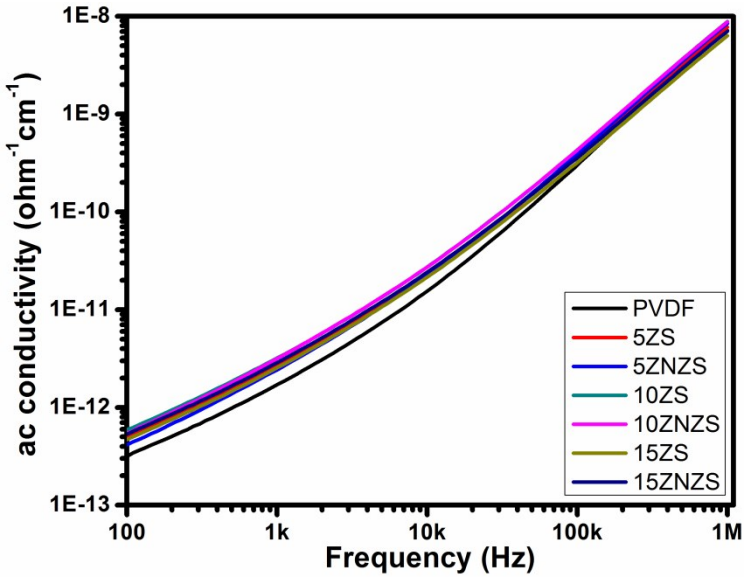

Fig. S6 Frequency dependent ac conductivity of all the composite films.

Fig. S7

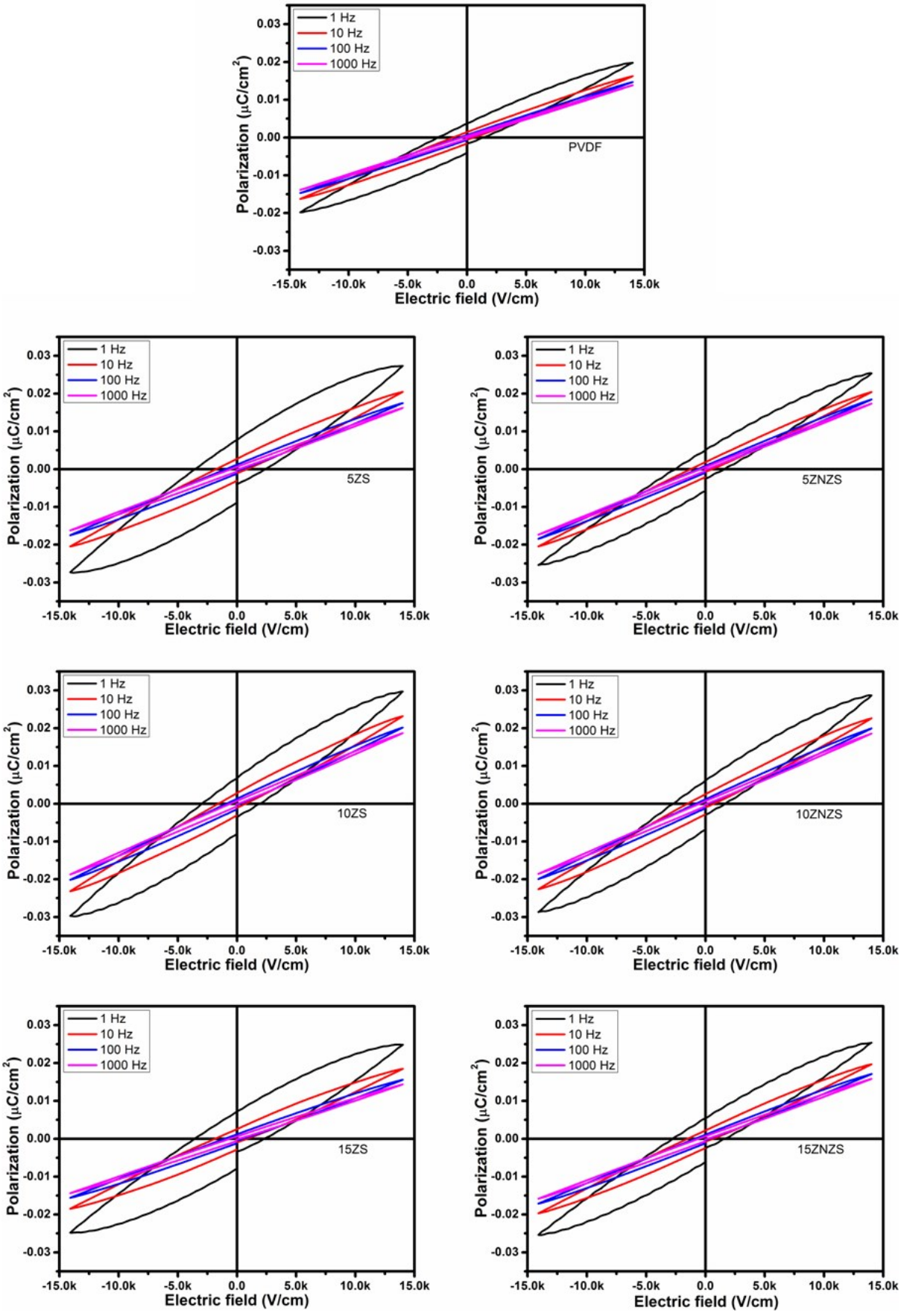

Fig. S7 P-E hysteresis loops of all the films at different frequency.

Discussion S4

ZS-PVDF films exhibited more amount of leakage current which after being added with real displacement current, gave more D_r value. Whereas, for PVDF-ZNZS samples, leakage current reduced significantly (Fig. S8) and as a result there was very faint leakage current to be added with real displacement current. Due to this reason, shrinkage of D-E loops for PVDF-ZNZS samples compared to that of PVDF-ZS films occurred.

Fig. S8

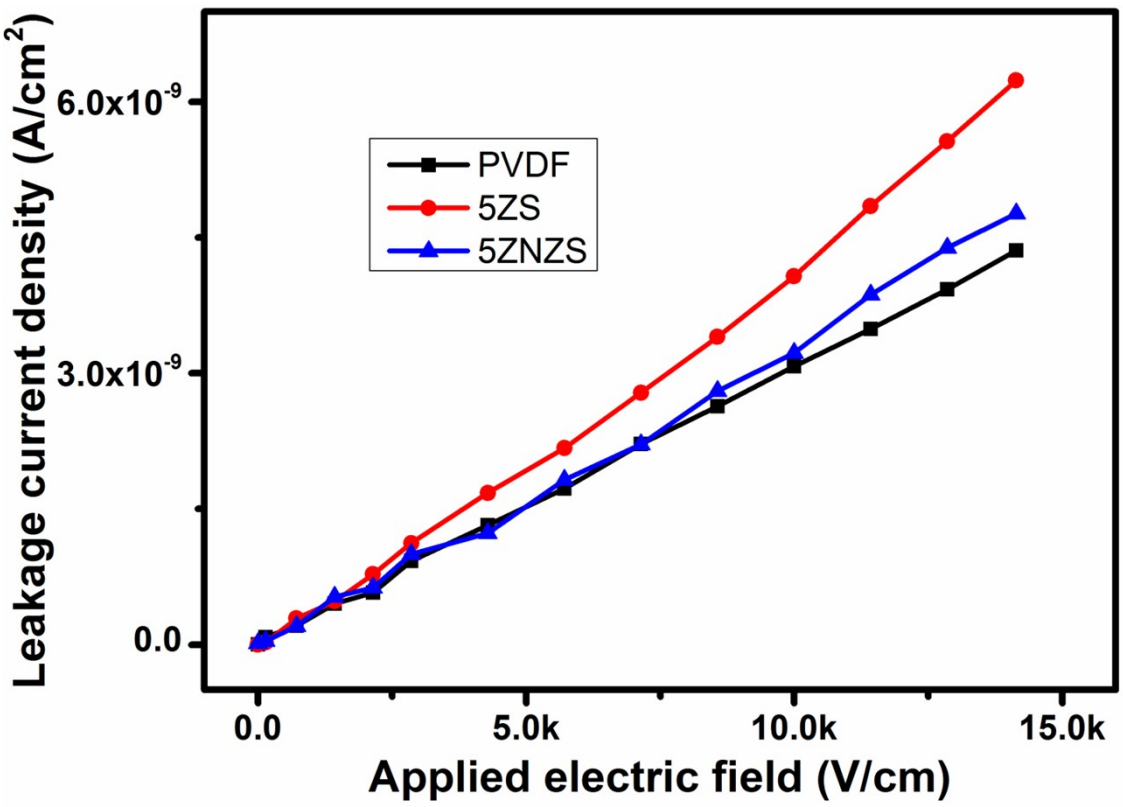

Fig. S8 Applied electric field dependent leakage current density of PVDF, 5ZS and 5ZNZS films.

Table S2

Table S2 Relation between input mechanical stimuli and piezoelectric output V_{OC} of 10ZNZS nanogenerator device.

Type of input stress	Pressure (kPa)	Frequency (Hz)	Output V_{OC} (V)
Repeated	1		8
human	2		13
finger	3	5	17
tapping and	4		23
releasing		1	22
		3	22
	4	5	23
		7	23

Fig. S9

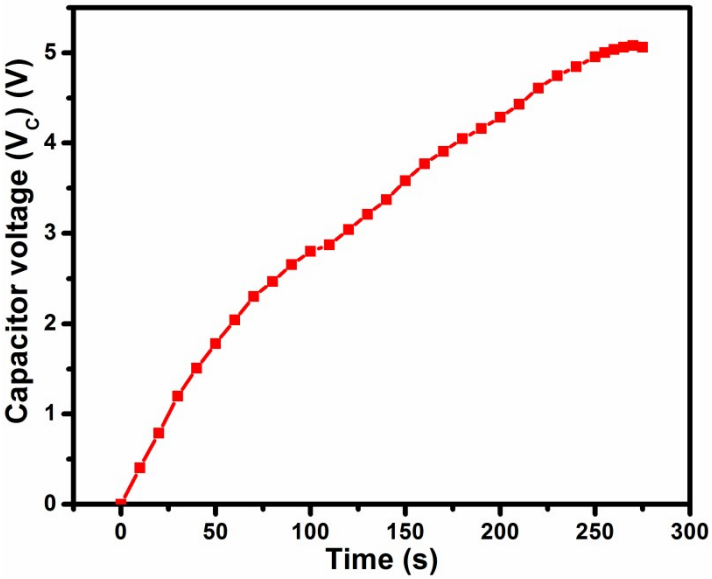

Fig. S9 Variation of capacitor charging voltage (V_C) with the variation of the duration of applied mechanical stress.

Fig. S10

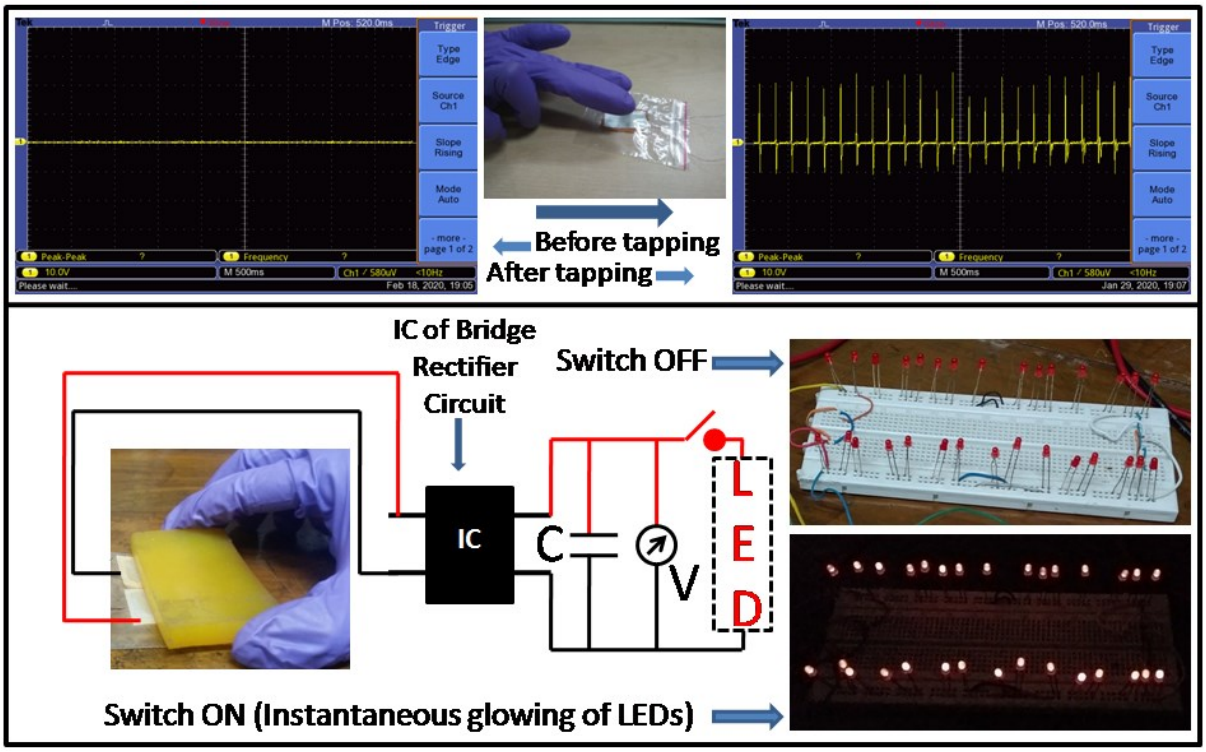

Fig. S10 Experimental setup for open circuit output voltage (V_{OC}) measurement and capacitor charging followed by LED glowing.

Fig. S11

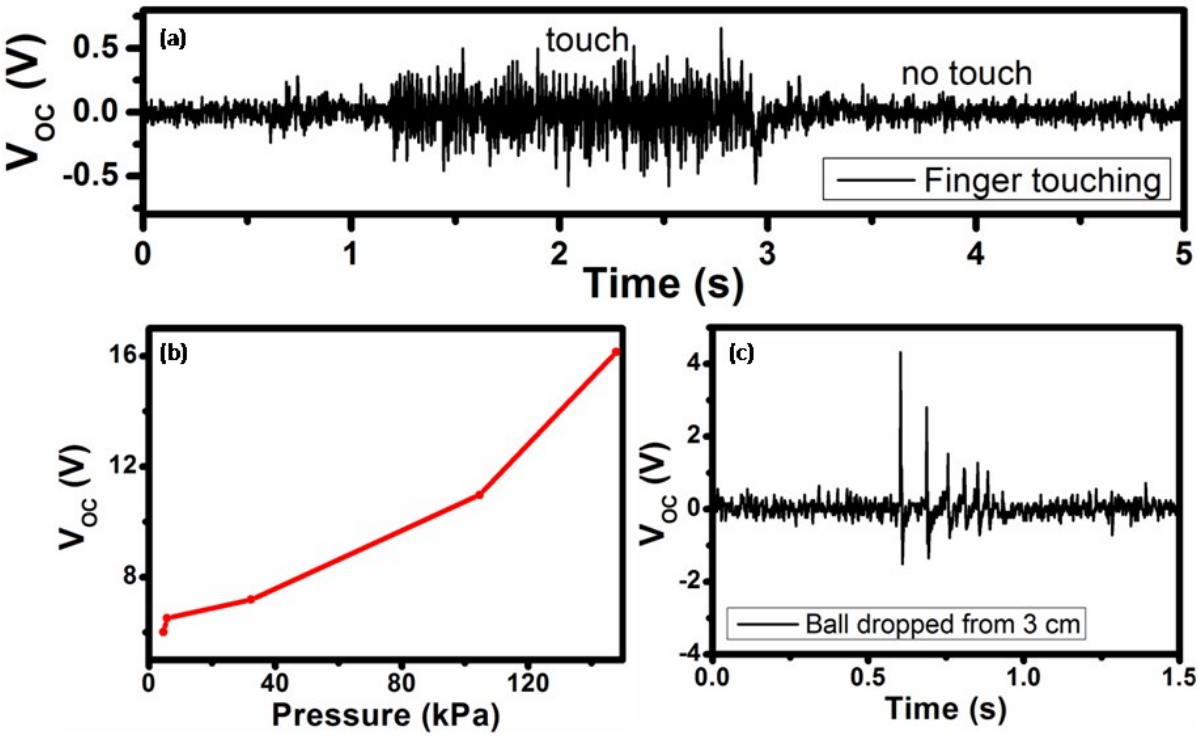

Fig. S11 (a) Output signal from HNG after normal finger touch. (b) Variation of V_{OC} with calculated pressure for ball dropping experiment from different height. (c) Output signal for repeated dropping and re-bouncing of the ball for a particular ball dropping experiment.

Table S3

Table S3 The relation of output V_{OC} from the HNG device with different types of input mechanical stimuli

Repeated human finger tapping								
Applied pressure (kPa)	1	2	3	4	4			
Frequency (Hz)	5				1	3	5	7
Output V_{OC} (V)	30	33	36	40	39	39	40	40
Walking on the device								
Weight of the man (kg)	70 (slow walking)			70 (fast)		50 (fast)		
Output V_{OC} (V)	6			6		2.7		
Δt of V_{OC} (s)*	1.3			0.7		0.7		
Rolling of cylinder on the device								
Weight (g)	20				100			
Speed (cm/s)	10		50		10		50	
Output V_{OC} (V)	3.47		3.72		5.18		6.53	
Δt of V_{OC} (s)	0.25		0.10		0.25		0.10	
Rubber ball dropping on the device								
Weight (g)	20							
h (cm)**	3		10		20	50		100
Output V_{OC} (V)	5.92		6.62		7.42	11.25		16.07
Dropping of light piece of paper on the device								
Weight (g)	0.05			0.25		0.50		
h (cm)	3							
Output V_{OC} (V)	2.2			2.6		3.3		

* **Δt** = the separation between positive and negative peaks of V_{OC}.

** **h** = height from where the object was dropped.